

# HELIOSTAT TESTING AT A NEW FACILITY IN SONORA, MEXICO

**Camilo A. Arancibia-Bulnes<sup>1,2</sup>, Manuel I. Peña-Cruz<sup>1</sup>, David Marroquín-García<sup>1</sup>, Rafael E. Cabanillas<sup>2</sup>,  
Carlos A. Pérez-Rábago<sup>1,3</sup>, David Riveros-Rosas<sup>4</sup>, Jesús F. Hinojosa<sup>2</sup> and Claudio A. Estrada<sup>1</sup>**

<sup>1</sup> Centro de Investigación en Energía, Universidad Nacional Autónoma de México. Priv. Xochicalco s/n Col. Centro, Temixco 62580, Morelos, México. Phone +52(55)56229791, e-mail address: caab@cie.unam.mx

<sup>2</sup> Departamento de Ingeniería Química y Metalurgia, Universidad de Sonora. Blvd. Luis Encinas y Rosales S/N, Col. Centro, Hermosillo 83000, Sonora, México

<sup>3</sup> IMDEA Energy, URJC-CAT, c/ Tulipán sn, 28933 Móstoles, Spain

<sup>4</sup> Instituto de Geofísica, Universidad Nacional Autónoma de México. Av. Universidad 3000, Ciudad de México, D.F., 04510 México.

## Abstract

A new facility known as Heliostat Test Field has been developed in Mexico. It consists of a solar tower, a laboratory, and 16 heliostats. Three different optical tests have been implemented for the evaluation of heliostats at this installation: sun tracking test, reflected spot test, and deflectometry test. These tests allow the evaluation of tracking, and slope errors of the heliostats. In particular, the later provides detailed slope maps of the reflecting mirrors.

Keywords: Heliostat; Central receiver technology; Deflectometry; Solar concentration.

## 1. Introduction

In the framework of a National Laboratory of Solar Concentrating and Solar Chemistry Systems, three research facilities were built in Mexico: a heliostat test field (HTF), a high radiative flux solar furnace [1], and an experimental photocatalytic water treatment plant. In particular, it was decided to build the HTF in the state of Sonora, one of the regions with the best insulations in Mexico. Developed jointly by *Universidad de Sonora* (UNISON) and *Universidad Nacional Autónoma de México* (UNAM), with partial financing from *Consejo Nacional de Ciencia y Tecnología* (CONACYT), the HTF is located 10 Km away from the City of Hermosillo (29°05'56"N 110°57'15"W, Fig. 1), in the campus of the Agriculture Department of UNISON. It is located near the southern edge of the Sonoran desert.

At the present stage, the purpose of the HTF is to serve as a platform for the development and testing of heliostat technology. It was finished and started up in December 2010. The installation consists of a 32 meters high tower, with a flat Lambertian target, 8 m × 6.7 m in size, for heliostat evaluation (Fig. 2). A room for the installation of thermal receivers was also built atop the tower, to be used in future stages of the project. In fact, this facility is the first stage of a larger project: a laboratory for research in central receiver technology, which will include the installation of 82 heliostats, to reach 2 MW thermal power [2].

Currently, there are 16 heliostats of different design installed in the HTF, most of them with 6 m × 6 m aperture area, and with facets canted to achieve 25 suns concentration ratio. The idea is to be able to test different heliostat technologies. For this purpose, different heliostat tests are being developed at the HTF. The purpose of this paper is to describe the new installation and to present preliminary results of the evaluation methods.



**Fig. 1. Location of the Heliostat Test Field.**



**Fig. 2. Picture of the HTF, showing a few heliostats, with the tower, and the laboratory at its base.**

## **2. Implemented Tests**

The operation of the HTF has been initiated with the implementation of three kinds of tests for heliostats: sun tracking test, reflected spot test, and deflectometry. All of them use an 8 bit Allied Pike camera to record images and MATLAB libraries for image processing.

### **2.1. Sun tracking test**

In the sun tracking test the heliostat is operated as a solar tracker. The central facet is removed from the heliostat and a camera is installed on its place, fixed perpendicular to the heliostat plane and pointing to the sun. In this way the camera tracks the sun together with the heliostat. The camera is fixed to the heliostat central beam, as close as possible to the gearbox, instead of fixing it to the mirror supporting structure, in order to reduce vibration with movement. Then, images from the sun are taken at regular intervals (Fig. 3). Images are processed in order to extract the coordinates of the center of the solar disc, measured in pixels,

over the CCD sensor. By taking into account the angular diameter of the sun and the number of pixels it covers, the position can be transformed from pixel coordinates into angles. The wandering of the solar disc image on the picture allows evaluating the tracking accuracy of the heliostat mechanism, by means of the standard deviation of the tracking error.



**Fig. 3. Typical image from a sun-tracking test.**

## 2.2. Reflected spot test

In the reflected spot test, the heliostat is used to reflect the sun rays to the Lambertian target (Fig. 4). The images produced on the target by the concentrating heliostat are recorded at regular intervals (Fig. 5). These pictures are processed to obtain the coordinates of the centroid of the produced solar image, at each time step. In this way the displacement of the solar image from the nominal target position can be evaluated, and standard deviations computed.

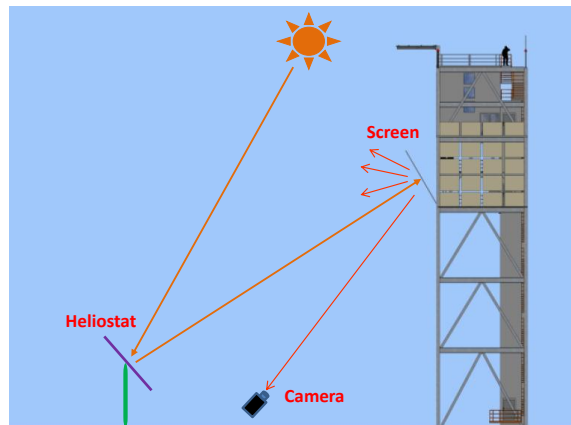


**Fig. 4. Experimental scheme for the reflected spot test.**

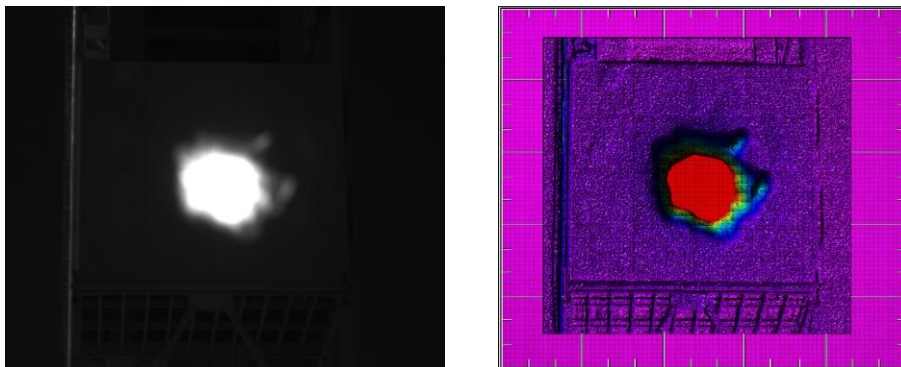


**Fig. 5. Typical image obtained during the reflected spot test (left), and the same picture after partial processing (right).**

### 2.3. Deflectometry test

In the deflectometry test, also known as fringe projection method [3,4], fringe patterns are projected at night on the Lambertian screen. Then, the heliostat is oriented in such a way as to reflect the image of the target and the fringes towards a camera located atop the tower (Fig. 6). Due to the mirror slope imperfections, the reflected fringes are distorted (Fig. 7). Therefore, from this distorted images it is possible to extract the slope errors to evaluate the reflecting facets of the heliostat.

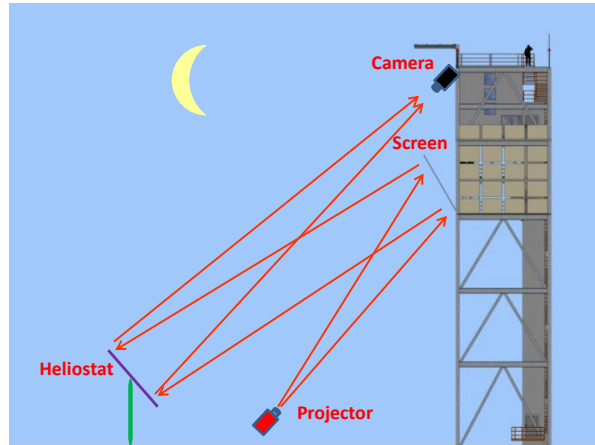


**Fig. 6. Experimental arrangement for the deflectometry test.**

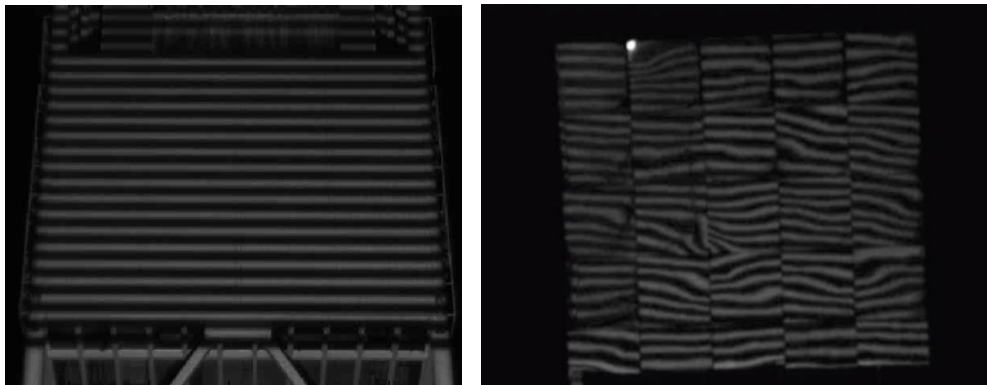


**Fig. 7. Pictures from the deflectometry test: fringes projected on the Lambertian screen (left), and after reflection by a heliostat (right).**

In particular the four step phase shifting method is used to extract the information. In this method, four sinusoidal patterns with fringes of equal frequency are projected on the screen successively. Each pattern differs from the preceding one by a  $\pi/2$  shift in the phase. Mathematically this is expressed by (for the case of horizontal fringes)

$$I_n(x, y) = A(x, y) + B(x, y)\cos[2\pi f y + \alpha_n]$$

where the  $I_n(x, y)$  is the intensity of the  $n$ -th pattern as a function of the  $(x, y)$  coordinates over the Lambertian target,  $f$  is the spatial frequency of the fringes ( $\text{m}^{-1}$ ), and the phase shift takes the values  $\alpha_0 = 0, \alpha_1 = \pi/2, \alpha_2 = \pi, \alpha_3 = 3\pi/2$ , for the four different patterns.

The four patterns, as seen by the camera after reflection by the heliostat, can be expressed as

$$\begin{aligned}
I_{r,0}(x, y) &= a(x, y) + b(x, y) \cos[\Phi(x, y)] \\
I_{r,1}(x, y) &= a(x, y) + b(x, y) \cos[\Phi(x, y) + \pi / 2] \\
I_{r,2}(x, y) &= a(x, y) + b(x, y) \cos[\Phi(x, y) + \pi] \\
I_{r,3}(x, y) &= a(x, y) + b(x, y) \cos[\Phi(x, y) + 3\pi / 2]
\end{aligned}$$

The phase  $\Phi(x, y)$  contains all the information of the geometry of the reflecting facets. This phase does not depend linearly with the  $y$  coordinate, as the original projected patterns did, but the functional relationship is arbitrary instead. To extract this function from the reflected patterns the following formula can be deduced from the preceding equations

$$\tan[\Phi(x, y)] = \frac{I_{r,1}(x, y) - I_{r,3}(x, y)}{I_{r,2}(x, y) - I_{r,0}(x, y)}$$

The phase  $\Phi(x, y)$  is said to be wrapped in this expression; it cannot be extracted simply by the arctangent function, because the tangent function is not biunivocal. Artificial phase jumps are introduced due to this fact when the arctangent function is used. These can be easily mistaken with phase jumps due to noise and other sources. To extract the phase correctly unwrapping algorithms are needed, that would be long to describe here [5]. In the present case a variation of Itoh's algorithm has been employed.

Once the phase is obtained, the local phase difference  $\Delta\Phi(x, y)$  with respect to a reference plane (ideal flat mirror) is calculated. The local angular deformation of the facets  $\delta(x, y)$  with respect to the flat surface is given by the following equation

$$\tan(2\delta) = \frac{\Delta\Phi}{2\pi f} \frac{Z_p - Z_f}{(Y_p - Y_f)^2 + (Z_p - Z_f)^2}$$

The quantities appearing in this equation are as depicted in Fig. 8. This particular formula is for the analysis of the vertical deformation in a heliostat located along the central axis of the field, by means of horizontal fringes, but it is easily extended to other cases.

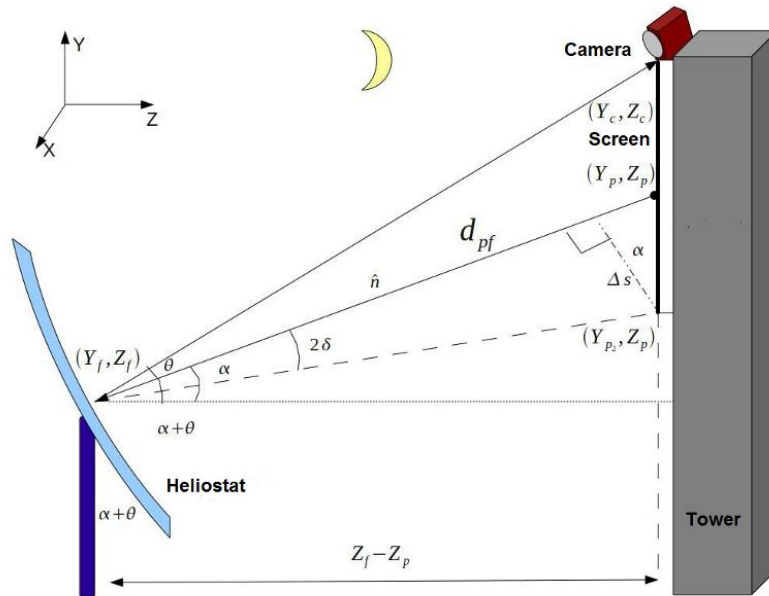
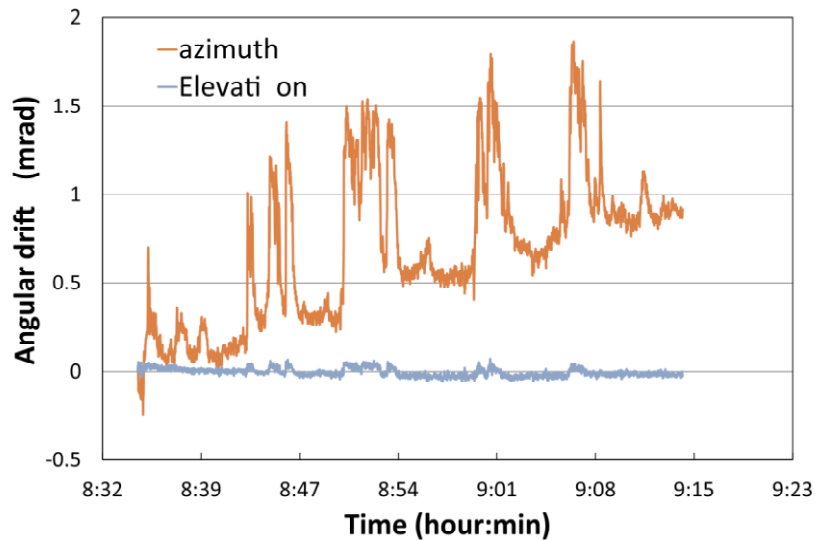


Fig. 8. Quantities involved in the mathematical analysis of deflectometry tests.

### 3. Results

In this section some examples of results obtained from the three implemented tests are discussed. In Fig. 8 a graph is presented for the sun tracking test. The data represent the angular deviation of the tracking during the test. As can be observed the elevation tracking worked very well in this particular run; i.e., the sun's image remained nearly static on the same vertical position on the CCD. On the other hand, the azimuth presented a very pronounced drift.



**Fig. 8. Angular drift in the azimuth and elevation axes as a function of time, for a sun tracking test.**

From the above, one can note that it is important to decouple the tracking errors caused by the accuracy of the mechanism, from those due to calibration errors in the tracking algorithm; i.e., random vibrations due to the mechanism need to be separated from the systematic error introduced by tracking calculation and calibration errors. This part of the process may be a subtle one. In the particular case presented, the drift in the azimuth direction is quite obvious, with almost linear behavior. Superposed on this, we can see several spikes due to wind loading, which are more characteristic of the backlash effect of the mechanism. Note that spikes in both tracking directions are clearly simultaneous, but those found in elevation are of much smaller amplitude. The amplitude of the spikes can be used to evaluate the tracking error due to the mechanism. For the particular case presented, a straight line is fitted to the azimuth data to represent the overall drift. Then, the standard deviation of the data with respect to this average behavior is calculated, to obtain the tracking error due to the mechanism. It is found that the standard deviation in the azimuth direction amounts to  $\sigma_t = 0.347$  mrad.

Another feature that can be observed in Fig. 8 is the presence of high frequency oscillations. However, they are not a reflection of the behavior of the mechanism. They are an artifact due to the pixel size of the camera, which limits the accuracy of the measurement.

In Fig. 9, results from a reflected spot test are presented. As well as in the previous test, drift spikes and high frequency oscillations can be observed. Similar information to the previous test could be extracted, but with the system acting as a heliostat instead of being used artificially as a solar tracker. Again, to analyze this information it would be necessary to separate the drift from the oscillatory behavior. It is interesting to note again the higher accuracy of the elevation as compared to the azimuth mechanism. This occurs because the first is a linear actuator, while the second is a worm gear and shaft mechanism.

The reflected spot test is potentially very interesting, as information of the shape of the solar image could be used for carrying out comparisons with ray tracing, which would help to further evaluate optical errors. This kind of comparisons will be implemented in the near future.

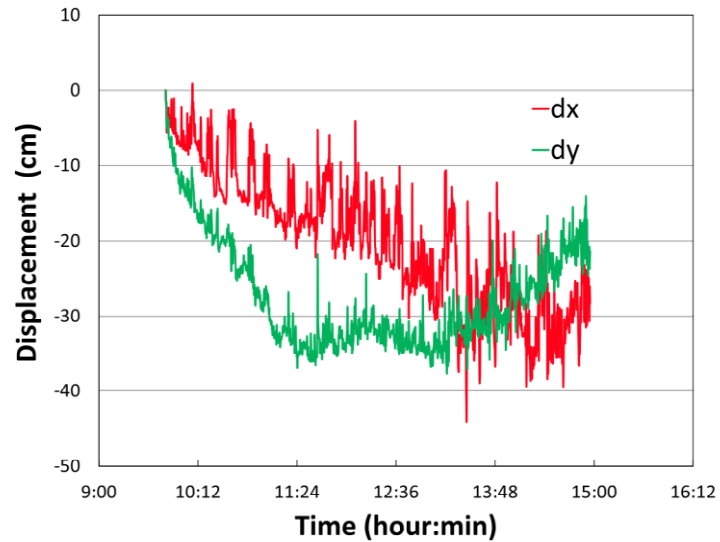


**Fig. 9. Reflected spot drift in the x and y axes as a function of time, for a sun-tracking test.**

Finally, in Fig. 10, an example of the results from the deflectometry test is shown. As can be observed, the test allowed determining the local deviation of the facet surface from the ideal planar geometry. A diagonal bending line can be observed at the center of the mirror, as well as stress points at the left side. From this data the standard deviation of the contour error was determined as  $\sigma_c = 1.90$  mrad, for this particular facet. Typical values found for other facets were closer to 1 mrad.

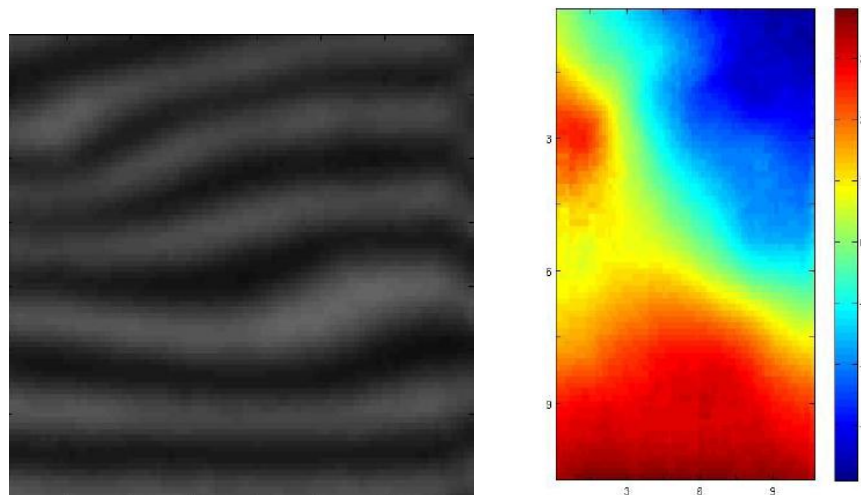


**Fig. 10. Image of fringes reflected by a mirror facet (left), and map of local angular deviations of the facet with respect to an ideal plane (right).**

#### 4. Conclusions

A new tower facility for the development and testing of heliostat technology has been established in Mexico.

This is the first installation of its kind in the country and in Latin America. Different kinds of heliostat tests, which complement each other, have been implemented or are being developed. This allows obtaining a variety of useful information of the heliostats under evaluation. Presently, tests to evaluate the tracking and slope errors of the heliostats are implemented. The latter, based on deflectometry techniques, provides detailed slope maps over the whole surface of the mirrors.

The first results of the tests allow us to evaluate the current heliostats in the field. We observe a better accuracy in the elevation tracking with respect to the azimuth tracking. Also we observe both stochastic and drift errors in the tracking, the stochastic error occurs with a standard deviation of 0.347 mrad. With regards to the deflectometry test, the implemented technique allows to get a map of the local deviation of the facet surface from the ideal planar geometry. The facets evaluated have a standard deviation between 1 and 2 mrad.

### **Acknowledgements**

This work has been funded jointly by CONACYT (Grants 56918 and 123767), Universidad de Sonora (UNISON), and Universidad Nacional Autónoma de México (UNAM). D. Marroquín-García and M. I. Peña Cruz, acknowledge CONACYT for graduate scholarships. C. A. Arancibia-Bulnes acknowledges UNISON for financial support during a sabbatical leave. R. Peón Anaya and P. Sosa Flores, from UNISON, are gratefully acknowledged for their technical support in heliostat installation, and in the implementation of the different tests. J.J. Quiñones Aguilar from UNAM is also acknowledged for technical support in equipment selection.

### **References**

- [1] D. Riveros-Rosas, J. Herrera-Vázquez, C. A. Pérez-Rábago, C. A. Arancibia-Bulnes, S. Vázquez-Montiel, M. Sánchez-González, F. Granados-Agustín, O. A. Jaramillo, C. A. Estrada, *Solar Energy*, 84 (2010) 792–800.
- [2] David Riveros, Carlos A. Perez-Rábago, Camilo A. Arancibia-Bulnes, Manuel Romero, Efraín Regalado, Rafael Cabanillas, Claudio A. Estrada. Sizing and performance analysis of a 2 MWth experimental solar heliostat field in Sonora. Proceedings of the 2009 Solar PACES symposium, Berlin, Germany.
- [3] C. E. Andraka, S. Sadlon, B. Myer, K. Trapeznikov, C. Liebner (2009). SOFAST: Sandia optical fringe analysis slope tool for mirror characterization. Proceedings of the 2009 Solar PACES symposium, Berlin, Germany. Article 15579.
- [4] S. Ulmer, T. März, C. Prah, W. Reinalter, B. Belhomme, *Solar Energy*, 85 (2011) 681–687.
- [5] D. C. Ghiglia, M. D. Pritt. (1989). *Two-Dimensional Phase Unwrapping: Theory, Algorithms, and Software*. Wiley, New York.